



Solar cell contacts: Quantifying the impact of interfacial layers on selectivity, recombination, charge transfer, and V_{oc}

Journal:	<i>Sustainable Energy & Fuels</i>
Manuscript ID	SE-ART-02-2021-000208
Article Type:	Paper
Date Submitted by the Author:	09-Feb-2021
Complete List of Authors:	Egelhofer Ruegger, Kira; University of Oregon, Chemistry and Biochemistry Roe, Ellis; University of Oregon, Physics Lonergan, Mark; University of Oregon, Chemistry and Biochemistry

ARTICLE

Solar cell contacts: Quantifying the impact of interfacial layers on selectivity, recombination, charge transfer, and V_{oc}

Kira E. Egelhofer Ruegger,^a Ellis T. Roe,^b and Mark C. Lonergan^{*a}

Interfacial layers (IFLs) are ubiquitous in solar cells, but their precise impact on carrier transfer rates and the relation of these rates to performance metrics and the concepts of selectivity and recombination is lacking. We report the use of a well-defined interdigitated back-contact (IBC) silicon solar cell to determine the precise role of such IFLs. We characterize the action of the common IFL spiro-OMeTAD by making it a third contact to the IBC cell. This architecture creates three solar cells within a single structure that, with numerical simulation, provide the exchange current densities (*i.e.*, charge transfer rates) for electrons (J_{on}) and holes (J_{op}) and the quasi Fermi-level splitting in the absorber, which measures the balance of generation and recombination. Further, we describe the relation of V_{oc} to contact recombination, the asymmetry in electron/hole collection rates at a single contact (contact selectivity), and the asymmetry in collection rates of the same carrier at separate contacts (carrier selectivity). Relative to bare gold, neat spiro-OMeTAD reduces J_{on} and J_{op} (their geometric mean $(J_{on}J_{op})^{0.5}$ decreases by 10^4), decreasing contact recombination. Addition of the common dopant Li-TFSI and air increase J_{op}/J_{on} by 10^6 with little effect on $(J_{on}J_{op})^{0.5}$, increasing contact hole selectivity. The significant increase in V_{oc} observed by introducing spiro-OMeTAD/Li-TFSI IFLs into the cells studied, however, is due to an increase in the carrier selectivity rather than the contact selectivity or recombination of the spiro-OMeTAD-modified contact. *Operando* measurements further show voltage-dependent changes in the J_0 s, demonstrating that spiro-OMeTAD contributes to hysteresis.

Received 00th January 20xx,
Accepted 00th January 20xx

DOI: 10.1039/x0xx00000x

Broader context

Solar cells operate by photogenerating excess charge carriers in an absorber material and, in competition with recombination, asymmetrically extracting them at so-called carrier-selective contacts, one that ideally collects only electrons and the other, only holes. Particularly in emerging photovoltaics such as perovskites, thin layers of organic semiconductors or related materials are introduced between the absorber and contact to improve power conversion efficiency. In terms of interfacial charge transfer, a prevailing view is that such interfacial layers improve performance by helping block the collection of the undesired carrier, considered a form of recombination. We use a novel platform to study the simultaneous impact of spiro-OMeTAD, a common interfacial layer, on the collection of electrons, the collection of holes, and on the recombination of electrons and holes. We quantitatively demonstrate that spiro-OMeTAD layers indeed passivate the contact toward recombination, but that larger improvements in the open-circuit voltage, a key cell metric, can come not only from this but also from increasing the asymmetry of the collection of electrons in the system. Further, *operando* measurements show transient changes in the properties of spiro-OMeTAD which suggest that it contributes to hysteresis phenomena commonly observed in perovskite and other solar cells.

Introduction

Photovoltaic action is a competition between the selective collection of photogenerated carriers (electrons and holes) and their recombination.¹ Selective collection occurs when one contact of the solar cell preferentially collects electrons and the other holes. This provides the asymmetry necessary to drive the

photovoltaic effect. A contact that collects one type of carrier with no restriction or energy loss while completely rejecting the other presents no limitations to the efficiency of a solar cell. Such a contact is perfectly selective, and it does not contribute to electron-hole recombination because it only collects one type of carrier.

The concept of a perfectly selective contact is well understood, but less so is the imperfect selective contact where both carriers are collected at some finite rate and neither without some restriction. In this case, what is the quantitative definition of selectivity? As the contact may now collect both carriers, how does the concept of selectivity relate to electron-hole recombination at the contact? How in turn do imperfect selectivity and contact recombination limit efficiency? These questions are addressed in recent theoretical models²⁻⁴ that

^a Department of Chemistry and Biochemistry, The Materials Science Institute, University of Oregon, Eugene, Oregon 97403, United States

^b Department of Physics, University of Oregon, Eugene, Oregon 97403, United States

† Electronic supplementary information (ESI) available. See DOI: 10.1039/x0xx00000x

ARTICLE

Journal Name

highlight the need for precise definitions and quantitative measures of selectivity and recombination, but these models have not been explored experimentally. Further, prominent solar cell technologies such as silicon⁵ and metal-halide perovskites⁶ are limited by their contacts. Consequently, there has been intense interest in improving solar cell contacts to the perfectly selective limit. This pursuit is often cast in terms of designing and developing carrier-selective contacts, but the term carrier selective is typically used without definition.

A common means of improving solar cell contacts is through the introduction of an interfacial layer (IFL) between the absorber and current collecting electrode.⁷ This is particularly true in emerging technologies based on perovskite and tandem absorbers/architectures.⁸⁻¹² As with solar cell contacts in general, performance enhancements are often qualitatively described in terms of selectivity or recombination or both, but their role in the action of IFLs remains unclear. For instance, the most recent and comprehensive review of IFLs⁷ states that “interfacial layers with appropriate energy levels are introduced to enhance the charge selectivity of the corresponding electrode by preventing unfavourable recombination...”. This statement connects decreased recombination with improved selectivity, the extreme limit of which is no recombination at a perfectly selective contact. But are selectivity and recombination really connected in an imperfect contact, or are they distinct, independent phenomena as others¹³ suggest?

The mechanistic ambiguity surrounding the terms selectivity and recombination as applied to IFLs is amplified by the fact that the action of IFLs is most often explored by their effect on parameters, such as the open-circuit voltage (V_{oc}),¹⁴⁻²⁵ that convolute recombination and selective carrier collection not just at a single contact but throughout the entire photovoltaic. Ultimately, the action of IFLs needs to be understood in terms of the fundamental rates of electron and hole transfer processes at the interface, as affected by, for instance, energy level shifts or the introduction of other charge transfer barriers. The interrelation between and action of IFLs on selectivity, recombination, and these interfacial electron and hole transfer rates remains a significant knowledge gap.

A prime example of where there is need for further mechanistic understanding is in describing the action of the most common hole selective IFL used in perovskite and solid-state dye-sensitized (SSDS) solar cells is 2,2',7,7'-tetrakis-(N,N-di-*p*-methoxyphenylamine)-9,9'-spirobifluorene (spiro-OMeTAD, Fig. 1).^{8,9,14-16,18,21,24,26,27} A contact modified with spiro-OMeTAD is commonly referred to as a hole selective contact.^{19,20,22,24,28} Its operation as such is primarily attributed to two interrelated factors. The first stems from the energy level alignments between the contact and the absorber. Photoemission spectroscopy studies show that spiro-OMeTAD introduces more significant charge transfer barriers to electron transfer relative to hole transfer when used with various perovskite absorbers.^{9,26} And while in these studies the effects of spiro-OMeTAD on the charge transfer rates are not quantified, the V_{oc} has been shown to change when the charge transfer barriers change.²⁶ The second factor is the effect of

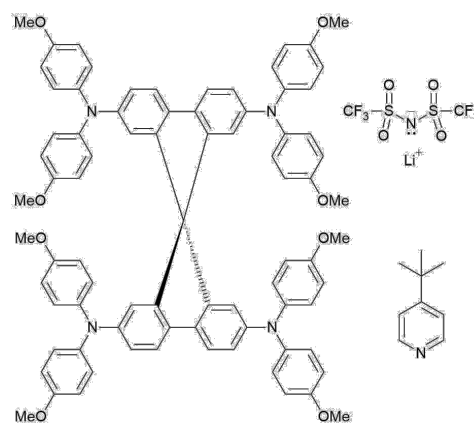


Fig 1 Structure of spiro-OMeTAD (left), Li-TFSI (top right), and t-BP (bottom right).

spiro-OMeTAD on the recombination of photogenerated charge carriers. Impedance spectroscopy and electroluminescence measurements have shown that spiro-OMeTAD can increase recombination resistance and reduce nonradiative recombination, respectively, relative to the unmodified gold electrode in perovskite solar cells.^{18,20} Furthermore, transient measurements of cell properties in SSDS cells have shown that common dopant bis(trifluoromethane)sulfoniimide lithium salt (Li-TFSI) affects recombination lifetimes.¹⁵

Changes in recombination lifetimes and energy level alignments are often related to the ability of the spiro-OMeTAD to block electrons,^{21,25,26} the “undesired” carrier, but the mechanisms by which this quality alters V_{oc} and its importance relative to other factors remains uncertain. Specifically, it is unclear whether changes in the collection of the undesired carrier are entirely responsible for changes in performance or whether modifications in hole collection also contribute. Hole processes have been shown to impact performance through low hole mobility in spiro-OMeTAD films, causing series resistance and thus degrading the fill factor.^{18,25} In fact, the importance of hole transport has been a common explanation for the need to dope spiro-OMeTAD (such as with Li-TFSI) because doing so increases the conductivity.^{14,15} However, this doping can also modify charge transfer barriers by shifting energy level alignments,²⁷ and hence could impact both electron and hole transfer at the interface. The relative importance of electron vs. hole transfer rates in determining performance, including how they relate to recombination and selectivity, is unknown.

The use of Li-TFSI in spiro-OMeTAD also introduces mobile ions, leading to its implication in hysteretic behavior.^{17,23,29-31} Pre-scan conditions and scan direction have been shown to affect the current-voltage characteristics of both SSDS and perovskite solar cells containing spiro-OMeTAD. There are mixed reports concerning whether spiro-OMeTAD contributes to hysteresis,²⁹⁻³¹ but Jacobs *et al.* show that ion accumulation in perovskite absorbers increases recombination at the absorber/spiro-OMeTAD interface and decreases hole injection from spiro-OMeTAD into the perovskite, indicating that spiro-OMeTAD does indeed play a role.²⁹ However, it is unclear whether these effects are caused entirely by ion accumulation in the absorber or if pre-scan light/voltage application (*i.e.*, cell

operation) changes the properties of spiro-OMeTAD itself as well. The effects of cell operation on the electron and hole transfer rates are simply unknown.

There are two primary goals of the work herein. The first is to measure electron and hole transfer rates at a solar cell contact and describe the relation of these rates to selectivity, recombination, and the important cell-level photovoltaic metric V_{oc} . The second is to advance understanding of the specific action of spiro-OMeTAD on modifying a metallic electrode and improving the V_{oc} of a solar cell. The two goals are synergistic in that the spiro-OMeTAD system is an excellent one to address the first because it can be widely tuned through air oxidation, the addition of Li-TFSI and *tert*-butyl pyridine (*t*-BP), and the application of bias. In turn, achieving the first goal provides exactly the fundamental understanding needed to mechanistically describe the action of spiro-OMeTAD including the effect of additives and cell operation.

Our unique approach uses a third contact to a commercially available interdigitated back-contact (IBC) silicon solar cell (the top contact, Fig. 2).^{32,33} This single structure provides three separate solar cells created from a lightly n-doped silicon absorber interfaced with either: (1) the top and n⁺ contacts, (2) the top and p⁺ contacts, or (3), the n⁺ and p⁺ contacts. In these three cells, the contact under study (the top contact) acts respectively as: (i) the hole contact, (ii) the electron contact, or (iii) a recombination center. All three cells may be simultaneously monitored *for the same film and during photovoltaic operation* to study the effects of environmental or pre-biasing conditions. Our ability to measure hole and electron processes and recombination simultaneously with the IBC cell, coupled with the capacity to accurately model such silicon-based cells using numerical simulation, makes it possible to determine exchange current densities (J_0 s) quantifying electron and hole transfer. Aided by additional insight from our recent theoretical model,^{2,3} these J_0 values can then be related to concepts of selectivity and recombination and to solar cell performance.

The use of a silicon model system is motivated by the unique opportunities presented by the IBC geometry, high quality versions of which are only available with a silicon absorber. Much as the general physics describing pn junctions, Schottky diodes, and other contacts are broadly applicable to a wide range of absorber materials, the connections we make between electron and hole transfer rates, the concepts of recombination and selectivity, and the V_{oc} are also broadly applicable. This of course is not without limit. For instance, organic solar cells possess unique contact physics because of the additional role of interfaces in separating the excitons that form in the low dielectric constant absorbers. Regarding spiro-OMeTAD specifically, the band-edge alignments of this system are different with silicon than they would be with other absorbers, in particular the perovskite system where it is most widely used. Here, however, we focus on how spiro-OMeTAD *modifies* a metal electrode – describing this physics will help guide the rational design of IFLs in general by elucidating how spiro-OMeTAD and its various additives and treatments (air, bias

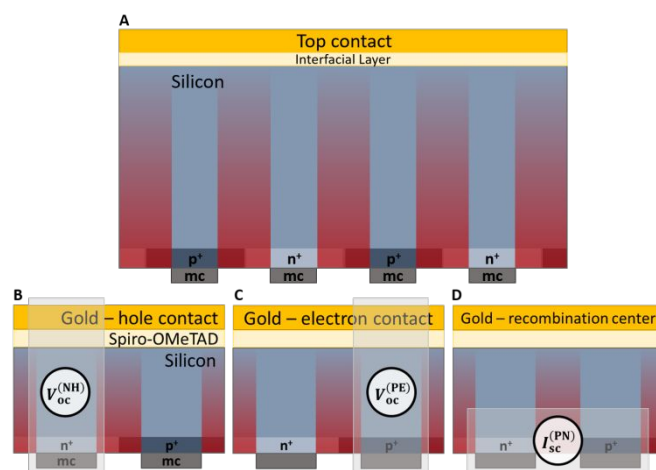


Fig 2 (A) Cross section of illuminated IBC cell structure³³ consisting of a lightly n-doped silicon absorber with interdigitated n⁺- and p⁺-Si contacts on the bottom and a third, spiro-OMeTAD-modified gold contact on the top. The cell is illuminated (indicated by areas of red to represent red light) through the interdigitated metal contacts on the back (labelled mc). The interfacial layer is a single layer consisting of either neat spiro-OMeTAD or a blend of spiro-OMeTAD, Li-TFSI, and *t*-BP. This structure contains three cells existing within a *single* solar cell, separated here to show the three electrical measurements used in this study: (B) the V_{oc} measured between the top contact and the n⁺ contact ($V_{oc}^{(NH)}$), (C) the V_{oc} measured between the top contact and the p⁺ contact ($V_{oc}^{(PE)}$), and (D) the short-circuit current measured between the n⁺ and p⁺ contacts ($J_{sc}^{(PN)}$). These quantities measure the modified contact's action as a hole contact, electron contact, and recombination center, respectively.

change electron and hole transfer relative to a pristine metal contact.

Experimental

Silicon IBC solar cells were generously donated by SunPower and chemo-mechanically polished by Axus Technology to remove the silicon nitride antireflective coating and pyramidal texturing for ease of thin film deposition. To begin device fabrication, Cr/Au electrodes were thermally evaporated onto glass slides (cleaned in detergent, sonicated sequentially in acetone and IPA, then spun dry), onto which IBC devices were mounted with Loctite Hysol 1C epoxy. Before epoxy attachment, copper wires were attached to the IBC cell n⁺- and p⁺-Si contacts using silver epoxy. Silver paint was used to make contact between these copper wires and the gold electrodes on the glass, and epoxy was used to protect metal components from further processing steps.

Completed devices were immersed for 10 minutes in a 50°C solution of 5:1:1 18.2 MΩ cm deionized water to 28.89% w/w NH₄OH_(aq) (Fisher Scientific, ACS grade) to 30% w/w H₂O_{2(aq)} (EMD Millipore, ACS grade), then rinsed with DI water and dried with nitrogen. Next, oxide was etched with buffered oxide etch (5:1 NH₄F_(aq) to HF_(aq), J.T. Baker/Avantor) for one minute. Neat spiro-OMeTAD (HPLC-grade, 99%, Sigma-Aldrich) films were spin coated onto the IBC cells in ambient conditions from 10 mg/mL solutions in chlorobenzene (HPLC-grade, 99.9%, Sigma-Aldrich) at 2000 rpm for 60 s to yield 3-5 nm films. Solutions were kept in air-free flasks under nitrogen and in the dark until spun cast, and filtered through 0.1 μm PTFE filters (GE/Whatman) directly before spinning. Salted solutions with

25% LiTFSI were made by adding 1.1 μL of a Li-TFSI (99.95%, Sigma-Aldrich) stock solution (107 mg/mL) in HPLC-grade acetonitrile (Fisher Scientific) and 0.7 μL *tert*-butyl pyridine (96%, Sigma-Aldrich) to a 0.2 mL solution of 10 mg/mL spiro-OMeTAD in chlorobenzene. Films from salted solutions were cast immediately after preparation of the solution unless otherwise indicated and again with filtration through 0.1 μm PTFE filters. Film thicknesses were measured using a Zygo NewView 7300 optical profilometer.

Gold electrodes (50 nm) were thermally evaporated and silver paint was used to create electrical contact to the top contact for characterization. Electrical measurements were performed using an Instec variable temperature vacuum/controlled atmosphere stage with 2.5 mm diameter aperture. Time course samples were first taken directly into an inert nitrogen atmosphere in the stage to establish a baseline for further measurements, and then re-exposed to air after 60 minutes to be measured in air over the next 6 hours.

A ThorLabs 785 nm laser diode with collimating lens and circularizing prisms was used as the illumination source. The light level was set by measuring a 2 mA short-circuit current between the n^+ - and p^+ -Si contacts of each freshly etched device before addition of a film or/and top contact. At this illumination intensity, the absorber is under high injection conditions. A Keithley 2400 source-measure unit and Keithley 7001 switching matrix were utilized to measure the $I_{sc}^{(PN)}$, $V_{oc}^{(NH)}$, and $V_{oc}^{(PE)}$.

Voltage step samples were fabricated in the exact same manner as time course samples but were measured in air over six hours before being taken into nitrogen for 90 minutes to establish a baseline for the *operando* measurements. Voltage was applied between the n^+ -Si contact and top contact for 60 seconds under illumination ($V_{app} = 0.8\text{ V}$, V_{oc} , 0 V, or -0.8 V) while keeping the p^+ contact at open circuit while also measuring the resulting current or voltage. The $V_{oc}^{(NH)}$, $V_{oc}^{(PE)}$, and $I_{sc}^{(PN)}$ were then measured for the next three hours.

Results

As shown in Fig. 2, we measure three quantities using the illuminated IBC cell to describe the contact under study: $V_{oc}^{(PE)}$, $V_{oc}^{(NH)}$, and $I_{sc}^{(PN)}$, all taken to be positive. The superscripts “p” and “N” refer to the p^+ - and n^+ -Si back contacts, respectively, while “H” and “E” refer to the top contact’s action as either the hole or electron contact when measured vs. the back n^+ - or p^+ -Si contact, respectively. The $I_{sc}^{(PN)}$ is the short-circuit current measured between the n^+ - and p^+ -Si contacts while $V_{oc}^{(NH)}$ and $V_{oc}^{(PE)}$ are the V_{oc} s measured between the top contact and the n^+ - or p^+ -Si contacts. First, we will introduce the qualitative meaning of these parameters then return to a more quantitative understanding through numerical simulation and theory below. We have previously used the IBC cell to characterize the effect of conjugated polyfluorenes on interfacial charge transfer, but only studied $V_{oc}^{(PE)}$ and $V_{oc}^{(NH)}$ in that work.³² The measurement of $I_{sc}^{(PN)}$ provides significant additional information on recombination.

The $V_{oc}^{(NH)}$ tells us about how the contact under study performs as the hole contact and $V_{oc}^{(PE)}$ as the electron contact.

The labels “hole contact” and “electron contact” should not be overinterpreted. Changes to $V_{oc}^{(NH)}$ and $V_{oc}^{(PE)}$ may signal changes in the effectiveness of the top contact as a hole or electron contact, respectively. However, this does not mean that the contact is necessarily becoming more efficient at collecting holes or electrons, respectively, because there are a variety of different rate processes that can lead to changes in V_{oc} .

The $I_{sc}^{(PN)}$ is a measure of the interfacial recombination at the top contact. If there is no interfacial recombination, $I_{sc}^{(PN)}$ is unaffected. As recombination at the contact increases, fewer electrons and holes are available for the p^+ - and n^+ -contacts to collect, thus decreasing the $I_{sc}^{(PN)}$. This is akin to measuring surface recombination velocities using transistor geometries.³⁴ We note that carrier diffusion lengths in the IBC cell are long enough^{33,35} for $I_{sc}^{(PN)}$ to be sensitive to changes in recombination of the top contact.

In this study we investigate the effects of thin (3-5 nm) films of neat and 25 mol% Li-TFSI-containing spiro-OMeTAD on the properties of gold contacts to IBC cells (full details in Methods). The complete action of spiro-OMeTAD layers in a solar cell depends on how they impact the optical properties of the entire cell, carrier transport through the cell, and charge transfer at interfaces within the cell. Our studies isolate the latter. We study thin spiro-OMeTAD layers to minimize limitations from bulk transport. The ability to study such thin films is made possible by the smoothness of the single crystal silicon substrate. To minimize optical effects,¹⁸ the cells are illuminated from the side opposite the top contact with a wavelength (785 nm) characterized by an absorption depth that is only a fraction of the absorber thickness. Spiro-OMeTAD films are spin coated onto IBC cells in ambient conditions and exposed to air for ten minutes before thermal evaporation of the gold contact and then for another ten minutes after contact deposition. To establish a baseline, samples are first held under nitrogen for an hour before being re-exposed to air for measurement every five minutes for six hours. Samples are kept in the dark except for the 4-5 seconds total required for each measurement of the three quantities $V_{oc}^{(PE)}$, $V_{oc}^{(NH)}$, and $I_{sc}^{(PN)}$.

Fig. 3 shows $V_{oc}^{(PE)}$, $V_{oc}^{(NH)}$, and $I_{sc}^{(PN)}$ measured over time in air. From Fig. 3a, it is immediately obvious that the addition of spiro-OMeTAD substantially increases the $I_{sc}^{(PN)}$ relative to gold regardless of whether Li-TFSI is present or whether the samples have been exposed to air. Thus, spiro-OMeTAD IFLs decrease the interfacial recombination of gold contacts. The addition of Li-TFSI increases the recombination compared to when it is not present as indicated by the decrease in $I_{sc}^{(PN)}$ from that of neat spiro-OMeTAD. After six hours of air exposure, the initial trend still holds.

Neat spiro-OMeTAD increases the $V_{oc}^{(PE)}$ of unmodified gold by $\sim 200\text{ mV}$ with a similar decrease in $V_{oc}^{(NH)}$ (Fig. 3b). Exposure to air has little additional effect. The incorporation of Li-TFSI causes a slight increase (decrease) in the initial $V_{oc}^{(NH)}$ ($V_{oc}^{(PE)}$). Exposure to air causes $V_{oc}^{(NH)}$ to increase by over 100 mV while $V_{oc}^{(PE)}$ decreases by about the same amount.

To investigate whether the charge transfer properties of the air-exposed Li-TFSI/spiro-OMeTAD/Au contact changes upon cell operation and could therefore contribute to hysteresis,

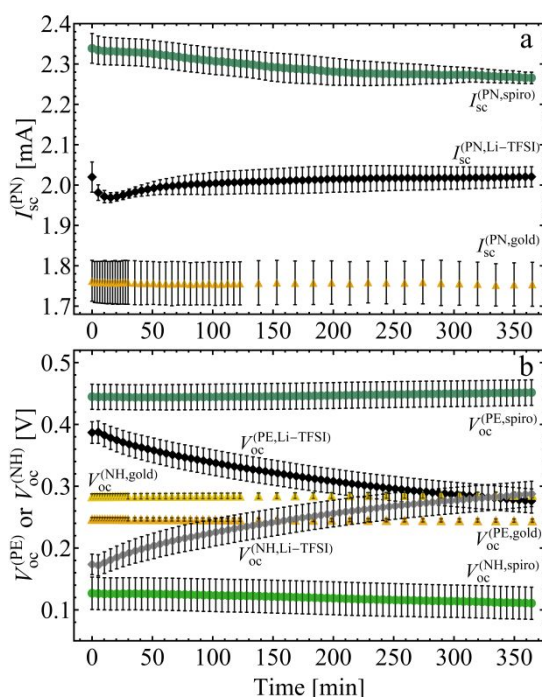


Fig 3 Experimentally measured (a) $I_{sc}^{(PN)}$ and (b) $V_{oc}^{(PE)}$ and $V_{oc}^{(NH)}$ values and their change over time in air for unmodified gold (yellow triangles), gold modified with neat spiro-OMeTAD (green circles), and gold modified with 25 mol% Li-TFSI spiro-OMeTAD (black/gray diamonds).

operando measurements were performed with Li-TFSI/spiro-OMeTAD operating as the hole contact vs. the n^+ -Si electron contact. Before conducting these measurements, the IFL/contact pair is exposed to air for six hours after which a nitrogen atmosphere is established for an hour for stabilization of $V_{oc}^{(PE)}$, $V_{oc}^{(NH)}$, and $I_{sc}^{(PN)}$. To operate the cell, it is illuminated for 60 seconds with the applied voltage (V_{app}) held at either: 0.8 V (forward bias), 0.34 V (V_{oc}), 0 V (short circuit), or -0.8 V (reverse bias). The cell is then returned to open circuit in the dark, and the time dependence of $V_{oc}^{(PE)}$, $V_{oc}^{(NH)}$, and $I_{sc}^{(PN)}$ is measured.

Fig. 4 shows the transients in $V_{oc}^{(PE)}$, $V_{oc}^{(NH)}$, and $I_{sc}^{(PN)}$ following cell operation. Although the cells are allowed to stabilize for 90 minutes after transition into nitrogen, some small drift in the measured quantities remains, thus data in Fig. 4 are corrected for this baseline drift (see Fig. S1 for originals, ES†). For each parameter, the direction of change is independent of the operating voltage, but the magnitude of change and the change over time depend on V_{app} . The largest changes occur when forward bias (0.8 V) is applied. The $V_{oc}^{(PE)}$ decreases while $V_{oc}^{(NH)}$ and $I_{sc}^{(PN)}$ both increase with each pre-bias application. Further, the duration of the effect depends on the voltage; voltages further into reverse bias cause longer relaxation times. In particular, reverse bias application (-0.8 V) leads to the most lasting effect of the voltages studied.

The IBC cell quantities we measure to describe the action of spiro-OMeTAD IFLs are all cell-level characteristics that depend on the balance of many different kinetic processes. However, our goal is to quantify how IFLs modify the kinetics of individual electron and hole processes at the interface and understand their relation to overall cell performance. To achieve this, we

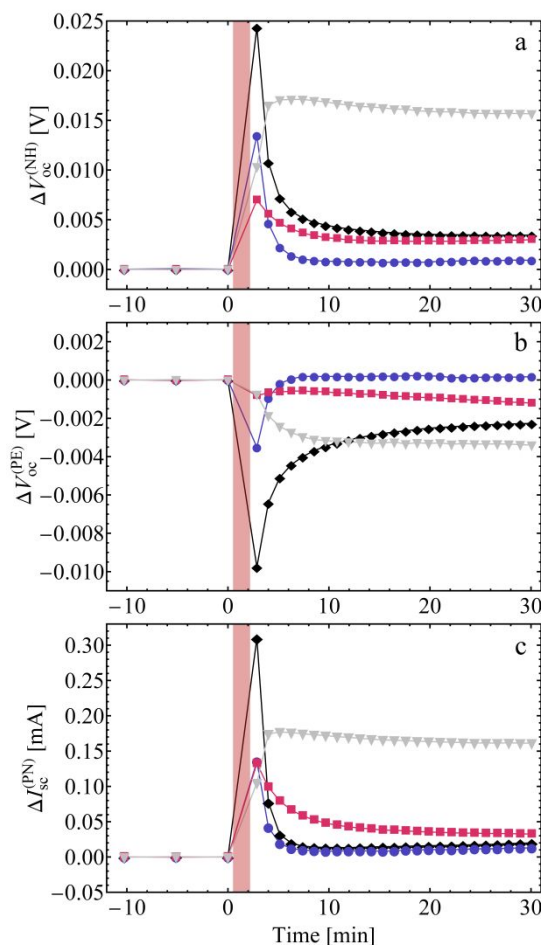


Fig 4 Changes to (a) $V_{oc}^{(NH)}$, (b) $V_{oc}^{(PE)}$, and (c) $I_{sc}^{(PN)}$ when potential steps are applied to the Li-TFSI-containing spiro-OMeTAD-modified gold contact when it acts as the hole contact (is measured vs. the n^+ -Si back contact). Black diamonds indicate forward bias $V_{app} = 0.8$ V, blue circles are $V_{app} = V_{oc}$, fuchsia squares are $V_{app} = 0$ V, and gray inverted triangles are reverse bias $V_{app} = -0.8$ V. The red shaded area indicates the time during which the voltage is applied under illumination.

use numerical simulation to connect the cell-level parameters $V_{oc}^{(PE)}$, $V_{oc}^{(NH)}$, and $I_{sc}^{(PN)}$ to the quasi-Fermi level splitting (QFLS) and to equilibrium exchange current densities, J_{0n} and J_{0p} , describing the rates of electron and hole transfer at the interface, respectively. Additionally, J_{0n} and J_{0p} provide a framework for understanding how concepts of selectivity and recombination limit solar cell performance.

Throughout, we use superscript labels to specify the contact or contacts associated with a particular quantity. We have chosen to label the top contact with either “E” or “H” to signify whether it operates as the electron or hole contact in a measurement. As the J_{0n} and J_{0p} values of the top contact do not depend on whether it is operating as an electron or hole contact, we simply omit the superscript. Hence, any time a J_0 value is presented without a superscript it should be considered that of the top contact.

COMSOL was used to model a 2D representation of the IBC cell including the top contact under study (complete details in ES†). We use boundary conditions described by diode expressions for the partial currents of electrons and holes, J_n

and J_p , at the interface between the semiconductor and the contact under study:

$$J_x = J_{0x} \left(e^{\frac{qV_x}{kT}} - 1 \right) \quad (1)$$

where q is the elementary charge, k is the Boltzmann constant, T is temperature, and $x = n$ (p) for electron (hole) processes. The quantity V_x is the difference in the quasi-Fermi level (*i.e.*, electrochemical potential) of the relevant carrier in the semiconductor and the Fermi level of the contact (there is no distinction between electron and hole Fermi levels in a metal). The quasi-Fermi level of a carrier in a semiconductor depends on its concentration. Under illumination, both the electron and hole concentrations are driven higher than their equilibrium values leading to their quasi-Fermi levels being different, and hence, the driving force for electron and hole transfer at the interface can be different, as measured by V_n and V_p .

Charge transfer at many semiconductor interfaces is described by eqn (1), including certain types of metal/semiconductor interfaces, pn junctions, and heterojunctions (see ESI† for a more detailed discussion).³⁵⁻³⁷ J_{0n} and J_{0p} enter into the simulations through these boundary conditions. The larger the J_0 , the faster the charge transfer rate. Simulations were performed by varying the J_{0n} and J_{0p} while solving for $V_{oc}^{(PE)}$, $V_{oc}^{(NH)}$, and $I_{sc}^{(PN)}$. Eqn (1) applies to interfaces based on semiconductors with free carriers including perovskites,³⁸ silicon, CdTe, and other crystalline absorbers.³⁵⁻³⁷

The first thing the simulations provide is an estimate of the QFLS in the absorber using $I_{sc}^{(PN)}$. Here, the QFLS is the difference between the electron and hole quasi-Fermi levels in the bulk of the absorber (at the point marked in the center of Fig. 2). The QFLS is determined by the balance of generation and recombination in the cell and is therefore sensitive to changes in interfacial recombination.³⁶ As the recombination decreases, the QFLS increases. As shown in Fig. 5, the simulated QFLS increases monotonically with the simulated $I_{sc}^{(PN)}$. Hence, these results confirm the qualitative idea mentioned above that $I_{sc}^{(PN)}$ measures interfacial recombination. The fact that the different colors lie on top of each other means that the QFLS is essentially independent of J_{0p}/J_{0n} . Further, the simulation data in Fig. 5 can be used to estimate the QFLS from the measured $I_{sc}^{(PN)}$.

Table 1 summarizes the IBC measurements and the QFLSs for the IFLs studied. Of course, the trends in QFLS with IFL composition and exposure to air are the same as described with $I_{sc}^{(PN)}$. The important new information is that in every case, the QFLS is significantly larger than either $qV_{oc}^{(PE)}$ or $qV_{oc}^{(NH)}$. The qV_{oc}

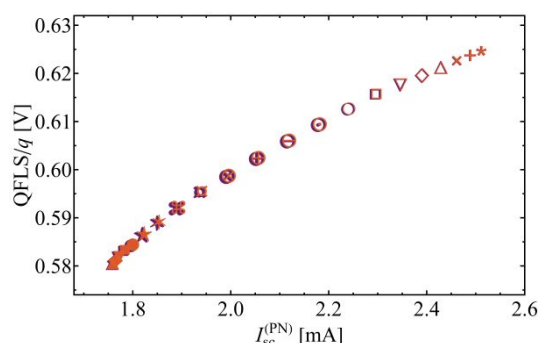


Fig 5 Simulation results demonstrating the relationship between the quasi-Fermi level splitting (QFLS) and the $I_{sc}^{(PN)}$ in the COMSOL model. The symbols indicate $(J_{0n}J_{0p})^{0.5}$ with values decreasing from bottom left to top right as a geometric series from 3.5×10^{-6} to 3.5×10^{-8} A/cm² with common ratio 1.3. Different colors represent different values of J_{0p}/J_{0n} (from 8×10^{-1} to 9.1×10^5) and stack on top of each other because the QFLS does not significantly depend on J_{0p}/J_{0n} .

of a solar cell cannot exceed the QFLS in the bulk; the fact that both qV_{oc} s are significantly lower indicates that they are not limited by recombination processes in the cell, as will be discussed further below.

The second thing the simulations provide is a measure of J_{0n} and J_{0p} , the fundamental parameters we use to describe how IFLs modify electron and hole transfer rates. It is useful to represent J_{0n} and J_{0p} in terms of their geometric mean, $(J_{0n}J_{0p})^{0.5}$, and ratio, J_{0p}/J_{0n} . The former describes how the IFL affects the combined rates of both electron and hole transfer. The latter describes how the IFL affects one rate compared to the other. In fact, J_{0p}/J_{0n} is taken as an intuitive definition of the contact hole selectivity (S_{con}) describing the relative rates of hole vs. electron transfer. The contact electron selectivity is defined as its reciprocal.

The significance of J_{0p}/J_{0n} and $(J_{0n}J_{0p})^{0.5}$ can be seen from the simulation results and considering the difference in V_{oc} s. Fig. 6 shows simulated values of $I_{sc}^{(PN)}$ versus $V_{oc}^{(PE)} - V_{oc}^{(NH)}$ for systematically varying values of J_{0p}/J_{0n} and $(J_{0n}J_{0p})^{0.5}$. Over a wide range of parameter space, the simulated $V_{oc}^{(PE)} - V_{oc}^{(NH)}$ and $I_{sc}^{(PN)}$ data form a nearly rectangular grid. A perfectly rectangular grid would indicate that $V_{oc}^{(PE)} - V_{oc}^{(NH)}$ and $I_{sc}^{(PN)}$ measure independent quantities. The curving over of the $I_{sc}^{(PN)}$ data at the bottom of the plot indicates the region of $(J_{0n}J_{0p})^{0.5}$ parameter space where bulk transport, rather than interfacial recombination, begins to limit the QFLS and therefore the $I_{sc}^{(PN)}$ (discussed further below). The direction of curvature is determined by the doping of the bulk silicon; when it is switched from lightly n- to p-doped the direction also changes. Fig. 6 shows that $V_{oc}^{(PE)} - V_{oc}^{(NH)}$ changes systematically with J_{0p}/J_{0n} but has little dependence on $(J_{0n}J_{0p})^{0.5}$. Hence, over a wide range of

Table 1. Experimental $V_{oc}^{(PE)}$, $V_{oc}^{(NH)}$, $I_{sc}^{(PN)}$, and simulation-generated QFLS data for unmodified gold, neat spiro-OMeTAD-modified gold, and Li-TFSI-doped spiro-OMeTAD-modified gold before (initial) and after (final) six hours of air exposure. The number in parenthesis is the uncertainty in the last digit.

	$V_{oc}^{(PE)}$ (V)		$V_{oc}^{(NH)}$ (V)		$I_{sc}^{(PN)}$ (mA)		QFLS at open circuit (eV)	
	Initial	Final	Initial	Final	Initial	Final	Initial	Final
Gold	0.247(3)	0.245(3)	0.283(4)	0.276(5)	1.76(5)	1.75(5)	0.580(5)	0.581(5)
Spiro	0.44(2)	0.45(2)	0.13(3)	0.11(3)	2.34(4)	2.27(1)	0.618(2)	0.614(1)
+ Li-TFSI	0.39(2)	0.28(2)	0.17(2)	0.29(2)	2.02(4)	2.02(2)	0.606(1)	0.609(1)

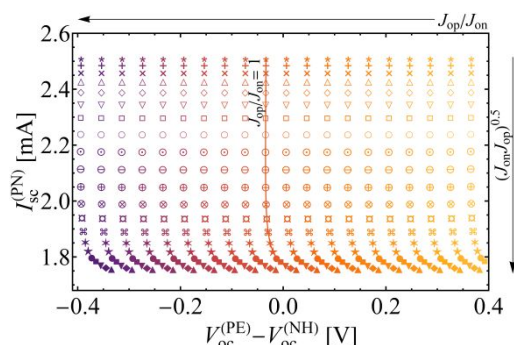


Fig 6 Simulation results for $V_{oc}^{(PE)} - V_{oc}^{(NH)}$ and $I_{sc}^{(PN)}$ as a function of J_{op}/J_{on} and $(J_{on}J_{op})^{0.5}$. The symbols indicate $(J_{on}J_{op})^{0.5}$ with values increasing from top to bottom as a geometric series from 3.5×10^{-8} to 3.5×10^{-6} A/cm² with common ratio 1.3. Data with the same values of J_{op}/J_{on} lie in quasi vertical groupings of the same color, for example as marked for the $J_{op}/J_{on} = 1$ data. The J_{op}/J_{on} increases from right to left as a geometric series from 1.5×10^{-7} (lightest orange) to 9.1×10^5 (darkest purple) with common ratio 4.7.

parameter space $V_{oc}^{(PE)} - V_{oc}^{(NH)}$ is a measure of contact selectivity; the comparison of the action of the contact as a hole contact vs. as an electron contact describes the asymmetry of hole vs. electron processes at the contact.

The $I_{sc}^{(PN)}$ changes systematically with $(J_{on}J_{op})^{0.5}$ but has little dependence on J_{op}/J_{on} for the range of parameter space and light intensity in the grid-like region of the simulation results. The net recombination rate at an interface with partial currents governed by eqn (1) depends on the excess carrier concentrations relative to those present at equilibrium. When both carrier concentrations have to be driven significantly from equilibrium to support recombination of the light current density (J_L), the net recombination rate is second order and is thus described by $(J_{on}J_{op})^{0.5}$.^{2,3} This is the situation we encounter because J_L is greater than both J_{on} and J_{op} in the grid-like region.

We compare the experimental values of $I_{sc}^{(PN)}$ and $V_{oc}^{(PE)} - V_{oc}^{(NH)}$ to the simulation data in Fig. 6 to find $(J_{on}J_{op})^{0.5}$ and J_{op}/J_{on} and hence to determine J_{on} and J_{op} (see ESI† for description of interpolation, simulation grid with points overlaid, and discussion of the unique aspects of the bare Au contact). Fig. 7 shows the J_0 values determined from this treatment. The background contour plot is described below. For now, consider that the direction of increasing recombination occurs in the direction of the dashed arrow labelled $(J_{on}J_{op})^{0.5}$ and the direction of increasing (decreasing) hole (electron) contact selectivity occurs in the direction of the dashed arrow labelled J_{op}/J_{on} .

The introduction of the spiro-OMeTAD, regardless of Li-TFSI or air exposure, decreases the $(J_{on}J_{op})^{0.5}$ by about four orders of magnitude. The introduction of Li-TFSI and subsequent exposure to air primarily change the contact selectivity: increasing J_{op}/J_{on} from 4×10^{-7} (quite electron selective) to 7×10^{-5} (still electron selective) and 0.3 (very slightly electron selective), respectively, but not to as high a value as gold itself (5×10^6 , quite hole selective). We also observed that when films were cast from Li-TFSI/spiro-OMeTAD solutions that had been aged, the J_{op}/J_{on} was observed to further increase with little change in the $(J_{on}J_{op})^{0.5}$ relative to the results for films prepared from fresh Li-TFSI/spiro-OMeTAD solutions (see the ESI†). Although the solutions were kept under an N₂ environment, the

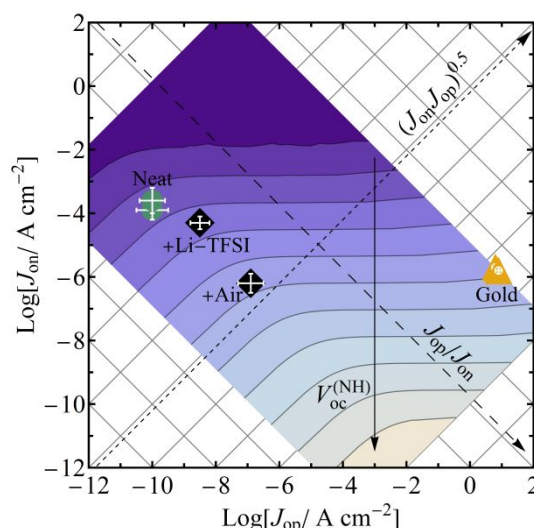


Fig 7 Contour plot of simulated $V_{oc}^{(NH)}$ values as a function of J_{on} and J_{op} . The $V_{oc}^{(NH)}$ contours increase by 0.05 V in the direction of the downward vertical arrow. The darkest purple region corresponds to $V_{oc}^{(NH)} < 0.05$ V and the tan region to $V_{oc}^{(NH)} > 0.55$ V. The locations of the experimental contacts are marked as symbols with error bars: gold triangles indicate bare gold, green circles indicate gold with neat spiro-OMeTAD, and black diamonds indicate gold with 25 mol% Li-TFSI spiro-OMeTAD, before and after six hours in air. The underlying grid shows constant values of $(J_{on}J_{op})^{0.5}$ and J_{op}/J_{on} increasing in the directions of the short- and long-dashed arrows, respectively.

observed changes in exchange current densities with solution age followed the same trend as air exposure of cast films; this is consistent with some oxidation of the spiro-OMeTAD in solution due to trace oxygen. Operation of the cell with air-exposed Li-TFSI/spiro-OMeTAD decreases both J_{op} and J_{on} , manifesting as a further decrease in $(J_{on}J_{op})^{0.5}$ and slight increase in J_{op}/J_{on} regardless of which voltage is applied.

The contour plot in the background of Fig. 7 addresses the relationship between the contact-level J_0 values and the cell-level device metric $V_{oc}^{(NH)}$. We consider the simulated $V_{oc}^{(NH)}$ data with the contact under study acting as the hole contact as is typical for spiro-OMeTAD-modified contacts. We first note that the QFLS, which is 0.58 to 0.63 eV over the entire simulated region, is always greater than $qV_{oc}^{(NH)}$. Next, there are two characteristic regions of the $V_{oc}^{(NH)}$ contour plot with all the spiro-OMeTAD contacts lying near the boundary between them. In the upper righthand region, the contours of equal $V_{oc}^{(NH)}$ run parallel to the J_{op} axis and perpendicular to the J_{on} axis; $V_{oc}^{(NH)}$ depends on J_{on} but not J_{op} . In the lower left region, conversely, the contours of equal $V_{oc}^{(NH)}$ run diagonally, parallel to the J_{op}/J_{on} contours and perpendicular to the $(J_{on}J_{op})^{0.5}$ contours; $V_{oc}^{(NH)}$ depends on contact selectivity but not on the geometric mean of the J_0 s.

The gold contact is clearly in the upper righthand region where $V_{oc}^{(NH)}$ depends only on J_{on} ; the spiro-OMeTAD contacts also remain very nearly within this region. This means that the primary reason that spiro-OMeTAD affects the $V_{oc}^{(NH)}$ in the IBC cell is a change in J_{on} . In Fig. 7, one can move from the $V_{oc}^{(NH)}$ of the gold contact to the $V_{oc}^{(NH)}$ value of any one of the spiro-OMeTAD contacts simply by changing J_{on} alone to move to the proper contour. Changing J_{op} has little to no additional effect on V_{oc} . In other words, all of the contacts to the IBC cell studied herein as hole contacts are approximated by:

$$V_{oc}^{(NH)} = \frac{kT}{q} \ln\left(\frac{J_L}{J_{0n}}\right) \quad (2)$$

where the J_{0n} is that of the spiro-OMeTAD-modified contact. The V_{oc} for the cell with the contact under study serving as the hole contact is determined by the rate of electron collection at this contact, and Li-TFSI/spiro-OMeTAD reduces the J_{0n} by up to about four orders of magnitude, depending on the level of oxidation determined by the amount of air exposure.

Discussion

We consider charge transfer at the interface in terms of thermionic emission, which can be applied to the description of both heterojunctions³⁷ and semiconductor/metal interfaces.³⁹ The J_0 for thermionic emission is given by:

$$J_{0x} = \kappa_x A_x^* T^2 e^{\left(\frac{-\phi_{bx}}{kT}\right)} \quad (3)$$

where A_x^* , κ_x , and ϕ_{bx} are the Richardson coefficient, transmission coefficient, and barrier height for electrons ($x = n$) and holes ($x = p$).³⁹ The IFL-modified interface can be viewed as a perturbed semiconductor/metal interface in which case the ϕ_{bn} and ϕ_{bp} are given by the difference between the contact Fermi level and conduction and valence band energies, respectively, of the absorber. The IFL in this case is seen as modifying the effective work function of the metal with any additional charge transfer barrier due to tunneling or additional band offsets being captured in κ . For a metal/semiconductor contact, κ is one, but it is generally less than one for molecular contacts with a lower density of states than a metal. In addition, the ϕ_{bn} and ϕ_{bp} of a semiconductor/metal contact sum to the band gap energy and changes in these quantities are typically equated with so-called work function effects. Alternatively, the IFL/contact can be considered in terms of a type I heterojunction where band offsets can be included in the ϕ_{bn} and ϕ_{bp} terms (see ESI† for a more detailed discussion). Either way, any shift in the energy levels or contact work function that causes an increase in one of the barriers would cause a decrease in the other. If an IFL causes only a change in ϕ_{bp} (and therefore ϕ_{bn}) and not κ , only the contact selectivity will be affected. Specifically, if ϕ_{bp} increases by Δ , J_{0p}/J_{0n} will change by a factor of $\exp[2q\Delta/kT]$ while $(J_{0n}/J_{0p})^{0.5}$ will remain unchanged.

The fact that spiro-OMeTAD significantly reduces $(J_{0n}/J_{0p})^{0.5}$ relative to gold indicates that the change is not simply a work function effect at a metal/semiconductor-like interface, but that the κ s also change due to the introduction of band offsets that present additional charge transfer or tunneling barriers. The spiro-OMeTAD layer itself is responsible for an overall reduction in $(J_{0n}/J_{0p})^{0.5}$ as evidenced by all of the IFLs falling on a similar $(J_{0n}/J_{0p})^{0.5}$ contour in Fig. 7. The addition of Li-TFSI and air oxidation tunes the J_{0p}/J_{0n} along this constant $(J_{0n}/J_{0p})^{0.5}$ contour the same way as changing the effective work function of the combined IFL/Au contact. The change in J_{0p}/J_{0n} from neat spiro-OMeTAD to air-oxidized with Li-TFSI corresponds to $\Delta = \sim 0.19$ V.

It is clear that spiro-OMeTAD changes the contact selectivity and $(J_{0n}/J_{0p})^{0.5}$, but we reiterate that the $V_{oc}^{(NH)}$ of the cells studied herein does not depend directly on these quantities. Rather, the $V_{oc}^{(NH)}$ depends only on the rate of electron collection (J_{0n}) as quantified by eqn (2). To better understand the origin of eqn (2), which is ubiquitous in solar cell physics, and its relations to selectivity and recombination, it is helpful to describe in general how contacts can limit the V_{oc} of a solar cell. This description is based on recent theoretical work by our group^{2,3} and by Kirchartz *et al.*;⁴ more details may be found there.

To start, we now consider two different types of selectivity: contact and carrier. Earlier, we defined contact selectivity as the ratio of the J_0 s of the two carriers at *one contact*, e.g., the hole contact selectivity $S_{con} = J_{0p}/J_{0n}$. Carrier selectivity (S_{car}) is instead the ratio of the J_0 s of the *same carrier* at the two contacts. For example, the electron carrier selectivity is defined as $S_{car,n} = J_{0n}^{(N)}/J_{0n}$. While S_{con} is useful in characterizing the J_0 values at a contact, the carrier selectivity is more important to the current density-voltage ($J(V)$) behavior because it describes the asymmetry available to support the QFLS in the cell.

The $J(V)$ behavior of a contact-limited solar cell depends on the carrier selectivity of both the electron and hole, but one typically dominates in the power quadrant. When, for example, the electron is limiting and J_L is greater than J_{0n} at both contacts, the V_{oc} is given by $(kT/q)\ln(S_{car,n})$. When J_L is between J_{0n} at the n^+ contact and J_{0n} at the top contact, there is excess carrier asymmetry in the system, and the contact-limited V_{oc} is given by $(kT/q)\ln(J_L/J_{0n})$. Herein, we refer to this latter situation as a light-limited carrier selectivity. Refer to the ESI† for a conceptual summary of how the $J(V)$ curve is related to carrier selectivity and Roe *et al.*³ for more details. If a cell is limited by contact recombination rather than by carrier selectivity, the V_{oc} is given by the QFLS/ q . When considering a cell with QFLS limited by recombination at the hole contact, $V_{oc} = (kT/q)\ln(J_L^2/(J_{0n}J_{0p}))$ when $J_L > J_{0p} > J_{0n}$ and $V_{oc} = (kT/q)\ln(J_L/J_{0n})$ when $J_{0p} > J_L > J_{0n}$. The two expressions come from recombination being second order vs. quasi-first order, respectively. Note that the latter yields the same expression as the light-limited carrier asymmetry expression, namely eqn (2).

The IBC cell measurements demonstrate that carrier collection asymmetry can be equally important as recombination in determining the impact of spiro-OMeTAD on V_{oc} . Although eqn (2) can hold in either case, the observation that the QFLS is always significantly greater than qV_{oc} for the cells studied herein shows that the V_{oc} is determined by the light-limited carrier selectivity. Though the spiro-OMeTAD-containing cells are not limited by recombination, the observed changes in QFLS demonstrate that spiro-OMeTAD IFLs do passivate the gold interface. The effect, however, is much smaller than on the light-limited carrier selectivity.

Recombination is often argued to be the primary mechanism by which spiro-OMeTAD increases the V_{oc} by as much as 400 mV in perovskite and SSDS solar cells.^{16,18-20} However, herein the QFLS/ q increases at most 40 mV in response to an almost four order-of-magnitude reduction in $(J_{0n}/J_{0p})^{0.5}$. This is partly because the full recombination effect of the gold electrode is limited by the bulk transport rates of both

carriers to the interface, evidenced by the curvature of the simulation data in Fig. 6 at low values of $I_{sc}^{(PN)}$. This curving over shows that a further increase in $(J_{0n}/J_{0p})^{0.5}$ eventually results in no change in $I_{sc}^{(PN)}$ and hence no further reduction in the QFLS. The $(J_{0n}/J_{0p})^{0.5}$ value for the Au contact puts it well into the bulk transport-limited regime, and similar bulk effects would be expected to limit the impact of contact recombination in other absorbers as well.³⁵ In general, we expect that large increases in V_{oc} well below the radiative limit are due to the effect of spiro-OMeTAD on the light-limited carrier asymmetry rather than on recombination. However, changes in the V_{oc} of cells that already have a relatively large V_{oc} could certainly be due to modifications to spiro-OMeTAD (e.g., Li-TFSI-induced oxidation) that affect recombination.

The discussion above highlights two important points about the role of selectivity in determining the V_{oc} . First, it is natural to separate the ideas of selectivity and recombination rather than thinking of recombination as a method to achieve selectivity. This is perhaps a semantic argument, but the distinct roles of the QFLS and carrier collection asymmetry in determining V_{oc} provide a natural basis for separating them. Second, altering the collection rate of the undesired carrier can be seen as either a selectivity or recombination effect. The impact of spiro-OMeTAD on collecting the undesired carrier has been previously recognized from impedance and transient photovoltage measurements on perovskite and SSDS cells^{14,15,25} and is often informally associated with qualitative ideas of recombination. The emphasis on recombination is understandable because the earliest form of eqn (2) is that derived from the classic treatment of radiative recombination,⁴⁰ with J_{0n} replaced with a J_0 quantifying the radiative recombination rate. However, the collection rate of the undesired carrier also contributes to the carrier selectivity (as defined herein), which can limit the qV_{oc} to less than the recombination-determined QFLS. The J_{0n} also alters the contact selectivity (as defined herein), but this is not as important to the $J(V)$ behavior of a contact-limited solar cell as the carrier selectivity.

The correlation of J_{0p}/J_{0n} , $(J_{0n}/J_{0p})^{0.5}$, or the individual J_0 values with a property such as V_{oc} as in Fig. 7 illustrates two additional important points. First, any measure of a contact property alone cannot provide a complete picture of the performance of an entire solar cell. That is, the J_0 values shown in Fig. 7 are characteristics of the contact, but the underlying contour plot that describes how they impact a cell level property such as V_{oc} depends on the properties of both contacts, the absorber, and the geometry of the cell. Both contacts are important because they define the carrier collection asymmetry necessary to achieve a photovoltaic effect and recombination anywhere in the cell limits the QFLS that can be obtained and ultimately harnessed to generate power. Second, it is difficult to determine the action of an IFL on a contact from measuring the V_{oc} of a solar cell. An excellent example comes from considering the Li-TFSI-containing samples herein. After extended air exposure ($t = 350$ in Fig. 3), the introduction of Li-TFSI/spiro-OMeTAD has almost no effect on $V_{oc}^{(NH)}$ (compare $V_{oc}^{(NH,Au)}$ and $V_{oc}^{(NH,Li-TFSI)}$ at $t = 350$ in Fig. 3). Thus, one might suspect there

is little work function modification or little general impact on charge transfer. Inspection of Fig. 7, however, shows this is not the case. The fact that the $V_{oc}^{(NH)}$ remains unchanged is a consequence of a cancellation of the effect on J_{0p}/J_{0n} , a “work function effect”, and a reduction in $(J_{0n}/J_{0p})^{0.5}$. The result is no change in J_{0n} , which is the relevant J_0 in the region where the contacts operate. A simple measurement of the V_{oc} such as in many studies of IFL-modified contacts¹⁴⁻²⁵ does not capture these important fundamental properties.

The same is true for studies of hysteresis in perovskite and SSDS solar cells that focus on changes to V_{oc} and other cell-wide parameters. Though some studies have employed other informative techniques^{17,28} for probing the movement of carriers and ions during solar cell operation and their relation to hysteresis, there is little information about whether there are fundamental changes to spiro-OMeTAD during cell operation and how these changes could contribute to hysteresis. Our *operando* measurements show that independent of the sign or magnitude of applied voltage, the J_{0n} and J_{0p} of Li-TFSI/spiro-OMeTAD/Au contacts both decrease in a transient manner when the cell is operated. These results indicate that the properties of the spiro-OMeTAD IFL change under the same conditions as those that produce hysteresis in complete cells and that the contribution of spiro-OMeTAD to hysteretic behavior is to reversibly decrease the rates of electron and hole transfer at the hole contact (decreasing $(J_{0n}/J_{0p})^{0.5}$ and slightly increasing J_{0p}/J_{0n}). These changes could occur in response to trap filling in the spiro-OMeTAD film,⁴¹ causing J_{0n} and J_{0p} to decrease regardless of the sign or magnitude of V_{app} , instead simply depending on the flow of some partial current across the interface. The reversibility of the effect could be due to the system relaxing back to equilibrium when V_{app} is removed through extraction of trapped carriers at the contact.

The changes in J_{0n} and J_{0p} due to operation of the cell in the power quadrant result in an increase in $V_{oc}^{(NH)}$, indicating that spiro-OMeTAD can contribute to the observed increases in V_{oc} that are often characteristic of hysteresis in both perovskite and SSDS cells. That the same direction of change also occurs when reverse bias is applied is in contrast to decreases in V_{oc} that are observed when complete cells are held at reverse bias before current-voltage characterization,²⁹ indicating that changes to spiro-OMeTAD itself likely compete with effects due to the absorber to produce hysteretic behavior. These results show a clear way in which spiro-OMeTAD IFLs can contribute to hysteresis.

Conclusions

Using the novel IBC platform, we have measured electron and hole transfer (J_{0n} and J_{0p}) at gold and spiro-OMeTAD-modified gold solar cell contacts and for the first time describe their relation to selectivity (J_{0p}/J_{0n}), contact recombination ($(J_{0n}/J_{0p})^{0.5}$), and V_{oc} . The addition of a thin spiro-OMeTAD interfacial layer between a silicon absorber and gold contact results in a four order-of-magnitude decrease in $(J_{0n}/J_{0p})^{0.5}$, which is largely unaffected by Li-TFSI or exposure to air. The addition of Li-TFSI and further air oxidation instead tune J_{0p}/J_{0n} over 6

orders of magnitude. A simple explanation for the observed behavior is in terms of a perturbed semiconductor-metal interface. The spiro-OMeTAD decreases the transmission coefficient for both electrons and holes relative to unmodified gold, and oxidation tunes the apparent work function of the contact resulting in a shift in the relative electron and hole transfer barriers. Operation of the cell results in further decreases in J_{0n} , J_{0p} , and $(J_{0n}J_{0p})^{0.5}$ and slight increases in J_{0p}/J_{0n} with more lasting changes occurring in reverse bias.

Overall, the reductions in $(J_{0n}J_{0p})^{0.5}$ demonstrate the passivation of the contact toward recombination, and the changes in J_{0p}/J_{0n} , by definition, shifts in the contact's selectivity. Although spiro-OMeTAD is normally considered a hole selective contact, when neat it actually makes gold electron selective at the Si interface. In the presence of Li-TFSI and air, spiro-OMeTAD-modified Au is more hole selective but never reaches the same hole selectivity as unmodified Au itself. That said, Li-TFSI/spiro-OMeTAD/Au can still result in a larger V_{oc} than pristine Au when operating as a hole contact due to a lower J_{0n} . The same is true for neat spiro-OMeTAD operating as an electron contact due to the reduction in J_{0p} . Upon cell operation, both J_{0p} and J_{0n} decrease, illustrating a clear way in which Li-TFSI/spiro-OMeTAD layers can contribute to $J(V)$ hysteresis in solar cells containing them.

We find that selectivity and recombination are separate effects in determining V_{oc} ; recombination is not a mechanism for altering selectivity. Further, both carrier and contact selectivities can be defined and influence cell response differently. Although the contact selectivity, J_{0p}/J_{0n} , and the complementary quantity $(J_{0n}J_{0p})^{0.5}$ are useful ways to express the effects of IFLs on a contact, they do not in general directly determine photovoltaic properties because such properties depend on the balance of all collection and recombination processes in the cell. For instance, for the junctions studied herein, V_{oc} depends only on the J_0 for the collection of the "undesired" carrier according to eqn (2) rather than on J_{0p}/J_{0n} . For spiro-OMeTAD, the undesired carrier is typically the electron and the action of spiro-OMeTAD in limiting its collection is typically equated with interfacial recombination. We show that spiro-OMeTAD indeed decreases recombination at the contact, but the dependence on J_{0n} as expressed by eqn (2) can arise from either a recombination effect or a carrier selectivity effect (or both). The latter is more important in the contacts studied herein; the carrier selectivity effect results in a much larger change in V_{oc} than the recombination effect, in part because recombination at a bare metal contact is already significantly limited by bulk transport in the absorber. Although perhaps best characterized by its effect on J_{0n} and J_{0p} , we find that in terms of selectivity and recombination the action of spiro-OMeTAD is twofold. It passivates the electrode resulting in an increase in the QFLS, and it increases the electron carrier selectivity thereby improving the cell's ability to fully extract the QFLS as V_{oc} . This fundamental insight is relevant across all photovoltaic technologies.

Conflicts of interest

There are no conflicts to declare.

Acknowledgements

This work was funded by the Division of Chemical Sciences, Geosciences, and Biosciences, Office of Basic Energy Sciences of the U.S. Department of Energy through DE-SC0012363. The authors also acknowledge support from the Rosaria Haugland Graduate Research Fellowship. This project utilized equipment in the SuNRISE Photovoltaic Laboratory in the Center for Advanced Materials Characterization in Oregon (CAMCOR), supported by the Oregon Built Environment and Sustainable Technologies (BEST) research center. The authors are grateful to SunPower for donating the IBC solar cells.

Notes and references

- 1 M.A. Green, Photovoltaic Principles, *Physica E*, 2002, **14**, 11-17.
- 2 E.T. Roe, K.E. Egelhofer, M.C. Lonergan, M.C. Limits of selectivity/recombination on the open-circuit voltage of a photovoltaic, *ACS Appl. Energy Mater.*, 2018, **1**, 1037-1046.
- 3 E.T. Roe, K.E. Egelhofer, M.C. Lonergan, Exchange current density model for the contact-determined current-voltage behavior of solar cells, *J. Appl. Phys.*, 2019, **125**, 225302-1-12.
- 4 T. Kirchartz, B.E. Pieters, K. Taretto, U. Rau, Mobility dependent efficiencies of organic bulk heterojunction solar cells: Surface recombination and charge transfer state distribution, *Phys. Rev. B*, 2009, **80**, 035334-1-6.
- 5 R.M. Swanson, "Approaching the 29% limit efficiency of silicon solar cells," *Conference Record of the Thirty-first IEEE Photovoltaic Specialists Conference*, 2005, Lake Buena Vista, FL, USA, 2005, pp. 889-894.
- 6 Z. Liu, L. Krückemeier, B. Krogmeier, B. Klingebiel, J.A. Márquez, S. Levchenko, S. Öz., S. Mathur, U. Rau, T. Unhold, T. Kirchartz, Open-circuit voltages exceeding 1.26 V in planar methylammonium lead iodide perovskite solar cells, *ACS Energy Lett.*, 2019, **4**, 110-117.
- 7 C.-C. Chueh, C.-A. Li, A. Jen, Recent progress and perspective in solution-processed interfacial materials for efficient and stable polymer and organometal perovskite solar cells, *Energy Environ. Sci.*, 2015, **8**, 1160-1189.
- 8 U. Bach, D. Lupo, P. Comte, J.E. Moser, F. Weissörtel, J. Slabec, H. Spreitzer, M. Grätzel, Solid-state dye-sensitized mesoporous TiO₂ solar cells with high photon-to-electron conversion efficiencies, *Nature*, 1998, **395**, 583-85.
- 9 H.-S. Kim, C.-R. Lee, J.-H. Im, K.-B. Lee, T. Moehl, A. Marchioro, S.-J. Moon, R. Humphry-Baker, J.-H. Yum, J.E. Moser, M. Grätzel, N.-G. Park, Lead Iodide Perovskite Sensitized All-Solid-State Submicron Thin Film Mesoscopic Solar Cell with Efficiency Exceeding 9%, *Scientific Reports*, 2012, **2:591**, 1-7.
- 10 C. Zuo, H.J. Bolink, H. Han, J. Huang, D. Cahen, L. Ding, Advances in Perovskite Solar Cells, *Adv. Sci.* 2016, **3**, 1500324.
- 11 Y. Wu, D. Yan, J. Peng, T. Duong, Y. Wan, S.P. Phang, H. Shen, N. Wu, C. Barugkin, X. Fu, S. Surve, D. Grant, D. Walter, T.P. White, K.R. Catchpole, K.J. Weber, Monolithic perovskite/silicon-homojunction tandem solar cell with over 22% efficiency, *Energy Environ. Sci.*, 2017, **10**, 2472-2479.
- 12 K.A. Bush, A.F. Palmstrom, Z.J. Yu, M. Boccard, R. Cheacharoen, J.P. Mailoa, D.P. McMeekin, R.L.Z. Hoyer, C.D. Bailie, T. Leijtens, I.M. Peters, M.C. Minichetti, N. Rolston, R. Prasanna, S. Sofia, D. Harwood, W. Ma, F. Maghadam, H.J. Snaith, T. Buonassisi, Z.C. Holman, S.F. Bent, M.D. McGehee,

- 23.6%-Efficient monolithic perovskite/silicon tandem solar cells with improved stability, *Nature Energy*, 2017, **2**, 17009.
- 13 E.L. Ratcliff, B. Zacher, N.R. Armstrong, Selective interlayers and contacts in organic photovoltaic cells, *J. Phys. Chem. Lett.*, 2011, **2**, 1337-1350.
- 14 Snaith, H.J., Grätzel, M. Electron and Hole Transport through Mesoporous TiO₂ Infiltrated with Spiro-OMeTAD, *Adv. Mater.*, 2007, **19**, 3643-3647.
- 15 A. Abate, T. Leijtens, S. Pathak, J. Teuscher, R. Avolio, M.E. Errico, J. Kirkpatrick, J.M. Ball, P. Docampo, I. McPherson, H.J. Snaith, Lithium salts as "redox active" p-type dopants for organic semiconductors and their impact in solid-state dye-sensitized solar cells, *Phys. Chem. Chem. Phys.*, 2013, **15**, 2572-2579.
- 16 J.-P. Correa-Baena, W. Tress, K. Domanski, E.H. Anaraki, S.-H. Turren-Cruz, B. Roose, P.B. Boix, M. Grätzel, M. Saliba, A. Abate, A. Hagfeldt, Identifying and suppressing interfacial recombination to achieve high open-circuit voltage in perovskite solar cells, *Energy Environ. Sci.*, 2017, **10**, 1207-1212.
- 17 S.A.L. Weber, I.M. Hermes, S.-H. Turren-Cruz, C. Gort, V.W. Bergmann, L. Gilson, A. Hagfeldt, M. Grätzel, W. Tress, R. Berger, How the formation of interfacial charge causes hysteresis in perovskite solar cells, *Energy Environ. Sci.*, 2018, **11**, 2281-2634.
- 18 N. Marinova, W. Tress, R. Humphry-Baker, M.I. Dar, V. Bojinov, S.M. Zakeeruddin, M.K. Nazeeruddin, M. Grätzel, Light harvesting and charge recombination in CH₃NH₂PbI₃ perovskite solar cells studied by hole transport layer thickness variation, *ACS Nano*, 2015, **9**, 4200 – 4209.
- 19 J. Lu, X. Lin, X., Jiao, T. Gengenbach, A.D. Scully, L. Jiang, B. Tan, J. Sun, B. Li, N. Pai, U. Bach, A.N. Simonov, Y.-B. Cheng, Interfacial benzenethiol modification facilitates charge transfer and improves stability of cm-sized metal halide perovskite solar cells with up to 20% efficiency, *Energy Environ. Sci.*, 2018, **11**, 1880-1889.
- 20 E.J. Juarez-Perez, M. Wußler, F. Fabregat-Santiago, K. Lakus-Wollny, E. Mankel, T. Mayer, W. Jaegermann, I. Mora-Sero, Role of the selective contacts in the performance of lead halide perovskite solar cells, *Phys. Chem. Lett.*, 2014, **5**, 680-685.
- 21 A. Dualeh, T. Moehl, M.K. Nazeeruddin, M. Grätzel, Temperature dependence of transport properties of Spiro-OMeTAD as a hole transport material in solid-state dye-sensitized solar cells, *ACS Nano*, 2013, **7**, 2292-2301.
- 22 P. Yadav, S.-H. Turren-Cruz, D. Prochowicz, M.M. Tavakoli, K. Pandey, S.M. Zakeeruddin, M. Grätzel, A. Hagfeldt, M. Saliba, Elucidation of charge recombination and accumulation mechanism in mixed perovskite solar cells, *J. Phys. Chem. C*, 2018, **122**, 15149-15154.
- 23 U.B. Cappel, T. Daeneke, U. Bach, Oxygen-induced doping of Spiro-OMeTAD in solid-state dye-sensitized solar cells and its impact on device performance, *Nano Lett.*, 2012, **12**, 4925-4931.
- 24 R.A. Belisle, P. Jain, R. Rasanna, T. Leijtens, M.D. McGehee, Minimal effect of the hole-transport material ionization potential on the open-circuit voltage of perovskite solar cells, *ACS Energy Lett.*, 2016, **1**, 556-560.
- 25 A. Dualeh, T. Moehl, N. Tetreault, J. Teuscher, P. Gao, M.K. Nazeeruddin, M. Grätzel, Impedance spectroscopic analysis of lead iodide perovskite-sensitized solid-state solar cells, *ACS Nano*, 2014, **8**, 362-373.
- 26 P. Schulz, E. Edri, S. Kirmayer, G. Hodes, D. Cahen, A. Kahn, Interface energetics in organo-metal halide perovskite-based photovoltaic cells, *Energy Environ. Sci.*, 2014, **7**, 1377-1381.
- 27 R. Schölin, M.H. Karlsson, S.K. Eriksson, H. Siegbahn, E.M.J. Johansson, H. Rensmo, Energy level shifts in spiro-OMeTAD molecular thin films when adding Li-TFSI, *J. Phys. Chem. C*, 2012, **116**, 26300-26305.
- 28 M. Yavari, M. Mazlou-Ardakani, S. Gholipour, M.M. Tavakoli, N. Taghavinia, H. Hagfeldt, W. Tress, Reducing surface recombination by a poly(4-vinylpyridine) interlayer in perovskite solar cells with high open-circuit voltage and efficiency, *ACS Omega*, 2018, **3**, 5038-5043.
- 29 D.A. Jacobs, Y. Wu, H. Shen, C. Barugkin, F.J. Beck, T.P. White, K. Weber, K.R. Catchpole, Hysteresis phenomena in perovskite solar cells: the many and varied effects of ionic accumulation, *Phys. Chem. Chem. Phys.*, 2017, **19**, 3094-3103.
- 30 E.L. Unger, E.T. Hoke, C.D. Bailie, W.H. Nguyen, A.R. Bowring, T. Heumüller, M.G. Christoforo, M.D. McGehee, Hysteresis and transient behavior in current-voltage measurements of hybrid-perovskite absorber solar cells, *Energy Environ. Sci.*, 2014, **7**, 3690-3698.
- 31 W. Tress, N. Marinova, T. Moehl, S.M. Zakeeruddin, M.K. Nazeeruddin, M. Grätzel, Understanding the rate-dependent J-V hysteresis, slow time component, and aging in CH₃NH₂PbI₃ perovskite solar cells: the role of compensated electric field, *Energy Environ. Sci.*, 2015, **8**, 995-1004.
- 32 C.D. Weber, D.P. Stay, M.C. Lonergan, Effects of Polyfluorene Polyelectrolyte Interfacial Layers on Selectivity and Recombination Measured Using the Interdigitated Back-Contact Solar Cell, *J. Phys. Chem. C*, 2016, **120**, 19951-19960.
- 33 W.P. Mulligan, M.J. Cudzinovic, T. Pass, D. Smith, N. Kaminar, K. McIntosh, R.M. Swanson, Solar cell and method of manufacture. U.S. Pat., 7897867B1, 2011.
- 34 S. Tiwari, D.J. Frank, S.L. Wright, Surface recombination in GaAlAs/GaAs heterostructure bipolar transistors, *J. Appl. Phys.*, 1988, **64**, 5009.
- 35 S.M. Sze, *Semiconductor Devices, Physics and Technology*, 2nd Ed., John Wiley and Sons, Inc., Hoboken, 2002.
- 36 P. Würfel, *Physics of Solar Cells: From Basic Principles to Advanced Concepts*, 2nd ed., Wiley-VCH, Weinheim, 2009.
- 37 K. Horio, Y. Yanai, Numerical modelling of heterojunctions including the thermionic emission mechanism at the heterojunction interface, *IEEE Trans. on Elec. Dev.*, 1990, **37**, 1093-1098.
- 38 A. Miyata, A. Mitioglu, P. Plochocka, O. Portugall, J.T.-W. Wang, S.D. Stranks, H.J. Snaith, R.J. Nicholas, Direct measures of the exciton binding energy and effective masses for charge carriers in organic-inorganic tri-halide perovskites, *Nat. Phys.*, 2015, **11**, 582-587.
- 39 E.H. Rhoderick, R.H. Williams, *Metal-Semiconductor Contacts*, 2nd ed., Oxford University Press, Oxford, 1988.
- 40 W. Shockley and H.J. Queisser, Detailed balance limit of efficiency of p-n junction solar cells, *J. Appl. Phys.*, 1961, **32**, 510-519.
- 41 J.A. Röhr, X. Shi, S.A. Haque, T. Kirchartz, J. Nelson, Charge transport in spiro-OMeTAD investigated through space-charge-limited current measurements, *Phys. Rev. Appl.*, 2018, **9**, 044017.